Erschienen in: Journal of Medicinal Chemistry; 61 (2018). - S. 5922-5933
https://doi.org/10.1021/acs.jmedchem.8b00105

Paradoxically, Most Flexible Ligand Binds Most Entropy-Favored: Intriguing Impact of Ligand Flexibility and Solvation on Drug–Kinase Binding

Barbara Wienen-Schmidt,[†] Hendrik R. A. Jonker,[‡] Tobias Wulsdorf,[†] Hans-Dieter Gerber,[†] Krishna Saxena,[‡] Denis Kudlinzki,[‡] Sridhar Sreeramulu,[‡] Giacomo Parigi,[§] Claudio Luchinat,[§] Andreas Heine,[†] Harald Schwalbe,*[,‡] and Gerhard Klebe*[,†]

[†]Institut für Pharmazeutische Chemie, Philipps-Universität Marburg, Marbacher Weg 6, 35032 Marburg, Germany

[‡]Institut für Organische Chemie und Chemische Biologie, Johann Wolfgang Goethe-Universität Frankfurt, Max-von-Laue-Straße 7, N160-3.14, 60438 Frankfurt am Main, Germany

[§]Magnetic Resonance Center (CERM/CIRMMP) and Department of Chemistry, University of Florence, Via Luigi Sacconi 6, 50019, Sesto Fiorentino, Italy

Supporting Information

ABSTRACT: Biophysical parameters can accelerate drug development; e.g., rigid ligands may reduce entropic penalty and improve binding affinity. We studied systematically the impact of ligand rigidification on thermodynamics using a series of fasudil derivatives inhibiting protein kinase A by crystallography, isothermal titration calorimetry, nuclear magnetic resonance, and molecular dynamics simulations. The ligands varied in their internal degrees of freedom but conserve the number of heteroatoms. Counterintuitively, the most flexible ligand displays the entropically most favored binding. As experiment shows, this cannot be explained by higher residual flexibility of ligand, protein, or formed complex nor by a deviating or increased release of water molecules upon complex formation. NMR and crystal structures show no differences in flexibility and water release, although strong ligand-induced adaptations are observed. Instead, the flexible ligand entraps more efficiently water molecules in solution *prior* to protein binding, and by release of these waters, the favored entropic binding is observed.

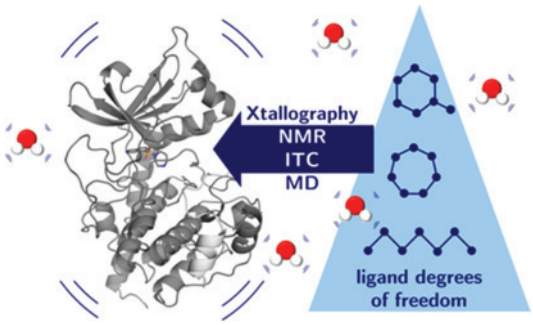

INTRODUCTION

Finding selective, effective, and clinically successful drugs is a long and expensive enterprise. Hence, it would be beneficial to accelerate this process by improving criteria to predict successful drug candidates and to identify inappropriate ones early on. Therefore, the analysis of parameters beyond affinity is required. In this context, thermodynamic analysis of protein–ligand interactions is used with increasing popularity. Accordingly, the design of drugs with certain thermodynamic properties has been described as a promising approach in many articles and reviews.[1−7] Moreover, design guidelines to accomplish purposefully tailored profiles have been intensely discussed, frequently advising the development of rigid, correctly preorganized ligands in order to influence the entropic penalty upon binding of the ligand to its target.[7−12]

However, there remains a lack of systematic studies that explore correlations between ligand structure, target protein characteristics, and thermodynamic signature. From our perspective, it is important to distinguish between the different characteristics of proteins. Particular factors that have to be taken into account are (1) size, (2) flexibility of the target, and (3) impact of water molecules. In this study, we investigated the wide and clinically relevant family of protein kinases. Protein kinases are highly flexible proteins as indicated by the presence of flexible loops in and next to the active site and helix movements upon ligand binding.[13−15] All protein kinases use ATP as phosphorylation reagent. This reagent transfers its terminal γ-phosphate group to an intermediately bound protein substrate, which is phosphorylated at a Ser, Thr, or Tyr residue. Kinases have been rarely investigated by means of comprehensive thermodynamic characterization. Only 10 unique kinases are listed in databases that are specialized for thermodynamic annotations, such as Scorpio[16] and BindingDB[17] (CDK2, ERK1/2, JNK2, Pim1, Aurora-A, thymidine kinase, nucleoside diphosphate kinase, vSrc, cSrc). Indeed for none of these targets has a systematic investigation of ligand series been conducted. Considering that, according to Manning et al., the human genome might encode for up to 518 protein kinases[18] and with respect to their importance as a

Received: January 21, 2018
Published: June 16, 2018

drug target class, there is a clear need for thermodynamic data to characterize protein kinases. The aim of this study is to start filling this gap in order to broaden our understanding of kinase dynamics and thermodynamics of ligand binding.

Here, the use of well-studied model proteins allows for the capture of extensive information from a wide range of experimental techniques. By use of the cAMP-dependent protein kinase (PKA) as a model system, elaborate information on protein−ligand interaction was obtained using X-ray crystallography, isothermal titration calorimetry (ITC), and nuclear magnetic resonance spectroscopy (NMR). The selected ligands are derived from the approved drug fasudil,[19] which has been developed as a rho-kinase inhibitor[20] but nonetheless displays nanomolar affinity toward PKA and blocks the ATP-binding site.[21] This site also accommodates the second substrate, the protein to be phosphorylated. In our studies, it is occupied by a fraction of protein, the inhibitory peptide PKI, comprising in our case 20 amino acids. It bears instead of the catalytically important serine an alanine residue; hence it cannot be phosphorylated in contrast to a physiological protein substrate. All of the studied fasudil-like ligands have equal atom count and comprise similar types of heteroatoms, but they vary in their internal degrees of freedom (Figure 1). In this way, the effect of ligand flexibility on the

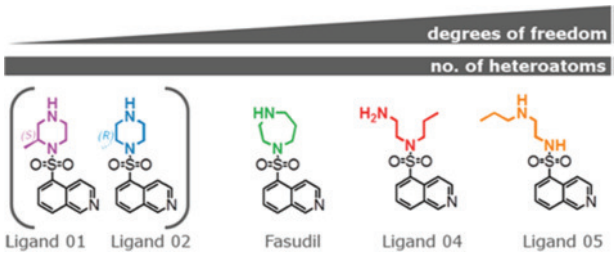

Figure 1. Chemical structure of the five ligands used in this study. From the left to the right the internal degrees of freedom increase and will, in any case, require an entropic price to be paid upon binding, as an increasing number of torsional degrees of freedom will be lost. In purple is the *S*-methylpiperazine-substituted fasudil derivative (ligand **01**). In blue is the *R*-methylpiperazine-substituted fasudil derivative (ligand **02**). In green is fasudil. In red is the open-chain fasudil derivative (ligand **04**). In orange is the long-chain fasudil derivative (ligand **05**). According to pK_a calculations all ligands will be protonated at their side chain amino group under the applied buffer conditions of pH 7.2 (not indicated in the formulas).

thermodynamic protein binding profile can be investigated. Thorough analysis of the underlying structural factors contributing to this thermodynamic profile has been made using X-ray crystallography and $^{1}H^{15}N$ best-TROSY (transverse relaxation optimized spectroscopy) NMR spectra. Furthermore, protein−ligand complex dynamics were analyzed using ^{15}N T_2 relaxation measurements. Additional insights about changes in the protein hydration pattern were obtained from water ^{1}H nuclear magnetic relaxation dispersion (NMRD) profiles by measuring the water proton relaxation rates. Here, we present a unique study where the static data from high resolution crystal structures are faced and combined with the information on the dynamics from detailed NMR measurements and complemented molecular dynamics (MD) simulations.

For the thermodynamic data, ITC was used to measure K_D and ΔH at chemical equilibrium. Subsequently, Gibbs free energy of binding ΔG and the entropic contribution $-T\Delta S$ were calculated using the following expression (eq 1):

$$\Delta G = \Delta H - T\Delta S = RT \ln K_D \quad (1)$$

Our study displays striking results that could hardly have been predicted, as counterintuitively the most flexible ligand binds entropically most favorably to the protein. Consequently, the hypothesis stating that a significant loss of ligand's degrees of freedom is, in all cases, entropically unfavorable to binding needs to be questioned and analyzed in the context of the entire binding event. We conclude that a generalization of simple design guidelines is not constructive and will not lead to satisfactory results.

RESULTS

Strongest Induced Fit Is Triggered by the Most Flexible Ligand. In order to determine the binding modes of all five ligands discussed, cocrystal structures were obtained. For all structures, resolutions between 1.4 and 1.6 Å could be achieved. In all five cases, difference electron densities are well-defined and indicate every heteroatom of the bound ligands (Supporting Information, Table S1) with 100% occupancy in the binding site. All structures have been deposited in the Protein Data Bank (PDB). The PDB codes are the following: ligand **01**, 5LCU; ligand **02**, 5LCT; fasudil, 5LCP; ligand **04**, 5LCR; ligand **05**, 5LCQ.

Importantly, the crystallographic data confirmed that all five ligands display a congruent hinge binding position of their respective isoquinoline moiety (Figure 2B). Moreover, their adjacent sulfonamides occupy a common orientation in all structures, where one oxygen points toward the glycine-rich loop (Gly-loop) and the second toward the hinge region. Hence, protein−ligand interactions are highly similar for the isoquinoline-5-sulfonamide portions of all five ligands. In all structures, a hydrogen bond is accepted by the isoquinoline nitrogen of the ligands provided by the backbone nitrogen of Val123 of the protein. Besides these interactions, the compounds' sulfonyl groups do not directly interact with the protein.

In contrast to the very similar ligand core binding, significant changes were noted among the five different protein−ligand complexes considering the substituents attached to the sulfonamide group.

In particular, the αG helix, the APE motif, and the position of the protein-kinase-inhibitor-peptide (PKI) are visibly shifted (Figure 2A). Yet, the most prominent difference was revealed in the active site. Here, the Gly-loop adopts three distinct positions ranging from a wide-open to a closed conformation when compared to the *apo*-protein (Figure 2B).

The first, most open position of the Gly-loop exhibits the structure with the open-chained ligand **04** (red). Here, the loop is pushed out of the ligand-binding site as the result of steric hindrance as the binding of ligand **04** requires more space in the area of the Gly-loop than any of the other ligands.

The second, half-open conformation of the Gly-loop is found in the structures of *S*-methylpiperazine-substituted ligand **01** (purple), the *R*-methylpiperazine-substituted ligand **02** (blue), and fasudil (green). Interestingly, all three ligands share a common position of the Gly-loop even though the interaction pattern of the homopiperazine moiety and 2-methylpiperazine moieties of the ligands with the protein differ significantly as will be described later.

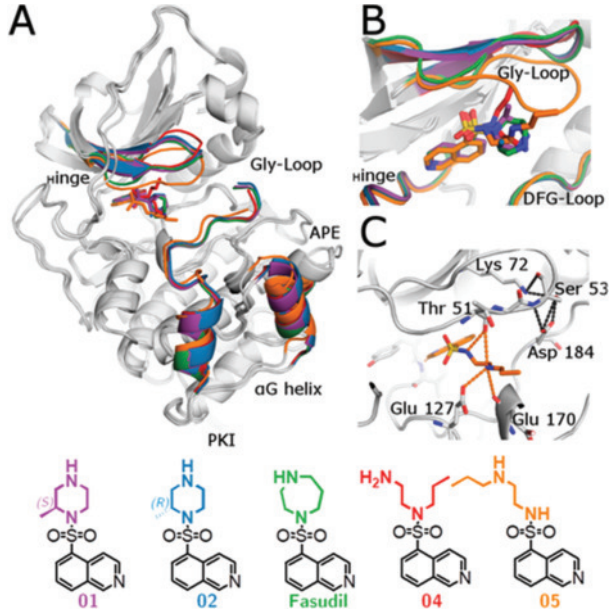

Figure 2. Superimposition of the cocrystal structures of all five ligands. (A) Overall view of the protein. Ligand **01** is displayed in purple, **02** in blue, fasudil in green, **04** in red, and **05** in orange. (B) Blow up of the active site. The long-chain ligand **05** induces the strongest conformational change, dragging the Gly-loop toward the ligand. (C) Interactions between **05** and the protein are displayed as orange dotted lines. The key interaction responsible for the downward movement of the Gly-loop is a hydrogen bond to Thr51. This transition is facilitated by the new interactions formed by the Gly-loop to the remaining part of the protein. The latter contacts are displayed as black dotted lines.

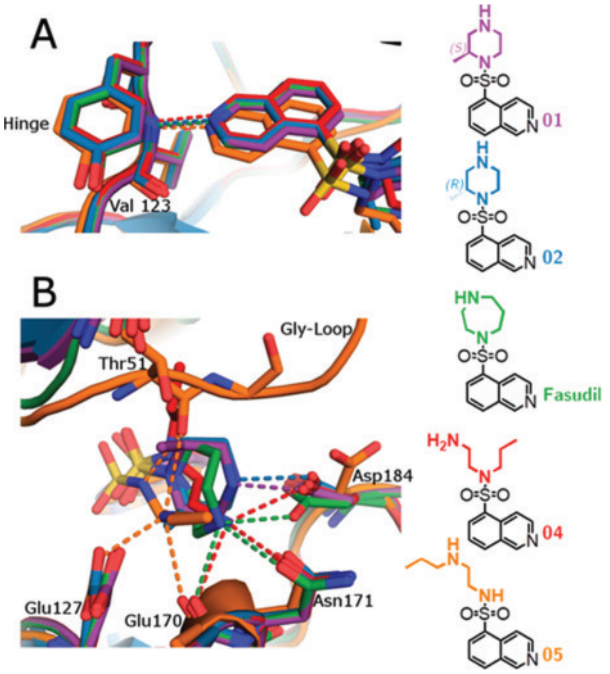

Figure 3. Polar interactions of all five ligands to the corresponding protein structures. Ligand **04** is displayed in red, fasudil in green, ligand **02** in blue, ligand **01** in purple, and ligand **05** in orange. Polar interactions are represented as dotted lines and colored in conformity with the corresponding ligand. (A) Interaction of the isoquinoline with the hinge region of the protein. (B) The five ligands form different polar interactions via their substituents attached to the sulfonamide group. In all cases the observed interaction pattern suggests that the terminal side chain amino group binds in protonated state (an itemized depiction of the binding modes is shown in Figure S1).

Finally, the third, closed state is depicted in the structure of the long-chain ligand **05** (orange). A strong induced fit resulting in a pulling-down of the Gly-loop can be observed. Responsible for this rearrangement are two hydrogen bonds formed between the backbone oxygen of Thr51 and the sulfonamide nitrogen as well as the secondary amine in the long chain of the ligand as shown in Figure 2C. Only in ligand **05** is a secondary amide present in the sulfonamide position, and it can hence act as a hydrogen-bond donor. All other ligands possess a tertiary amide in the sulfonamide, which does not have the ability to act as a hydrogen-bond donor. Consequently, the formation of the key interaction to Thr51 is impossible for all other compounds. In addition, steric hindrance would prevent the closed position of the Gly-loop for all ligands other than ligand **05**.

In the case of ligand **05**, the closed conformation of the Gly-loop is facilitated by additional interactions of the loop involving the neighboring amino acids of the protein: Asp184, Ser53, and Lys72. In total, five new interactions are formed (Figure 2C, black dotted lines).

From further analysis of the ligand binding mode, differences can be discerned with respect to the deviating substituents (Figures 3B and S1). The interactions established by the terminal amino groups differ; however, the observed H-bonding patterns suggest that in all ligands, this nitrogen binds as protonated ammonium group. The highest number of polar interactions to the protein is recognized by the homopiperazine portion of fasudil (green) and the terminal aminoethyl moiety of the open-chain ligand **04** (red). Interestingly, both ligands form comparable interaction patterns. In either case, the terminal amino group forms hydrogen bonds with the backbone carbonyl oxygen of Glu170 as well as the terminal carboxamide or carboxylate group of the side chains of Asn171 and Asp184. In contrast to fasudil (green) and **04** (red), the interaction pattern of the terminal aminoethyl nitrogen of the long-chain ligand **05** (orange) differs. The only common interaction occurs with the backbone carbonyl oxygen of Glu170. Furthermore, **05** interacts with the side chain of Glu127.

It is also notable that the *S*-methylpiperazine-substituted **01** (purple) and the *R*-enantiomer **02** (blue) each establish one hydrogen bond to Asp184 of the DFG-loop via their terminal NH group.

A difference in the position of water molecules of the residual hydration pattern can be observed for the different complexes. As a matter of fact, the protein flexibility takes impact on the observability of the adjacent water positions. By optimization of the diffraction quality of the studied crystals, the resolution of the collected data sets was improved. Nonetheless, many putative water molecule positions remained unresolved due to an ambiguous density distribution next to the region showing enhanced residual mobility in the crystal structure. A distinct analysis and quantification of the water molecule pattern and hence a comparison across the active sites of all complexes are limited due to the flexible nature of

the protein, which affects the diffraction pattern defining the electron density in this region.

The Most Flexible Ligand Binds Entropically Most Favored to the Protein. The thermodynamic signature of ligand binding to the protein was determined by ITC at pH 7.2. All profiles were assessed for putative buffer dependence to record possibly overlaid changes in protonation state upon complex formation. The selected buffers differ in their ionization enthalpy by approximately 30 kJ/mol.[22] A slope between −0.07 and −0.15 could be observed for fasudil, **04**, and **05** and +0.15 for **01** and **02** across the three considered buffers. We believe this scatter is insignificant within experimental accuracy. Accordingly, changes in protonation states upon complex formation can be excluded.

We assume all ligands adopt a protonated state in solution prior to protein binding and carry this state over to the protein-bound situation. This is in accordance with the observed interaction patterns in the crystal structures. Fasudil, **04**, and **05** have calculated pK_a values between 8.0 and 10.1, therefore definitely suggesting positively charged state in solution. The calculated pK_a value for the piperazine nitrogen of ligands **01** and **02** is 7.3, which is slightly below the applied buffer pH (calculated using http://www.chemicalize.org/, accessed Sep 9, 2015 and Sep 23, 2015). Hence, there might be a small partial proton uptake to reveal fully protonated state if compared to the slopes of the other compounds (see above). Even though we believe these differences are insignificant, we used for the evaluation of the thermodynamic signatures the profiles determined in phosphate buffer. This buffer exhibits very low ionization enthalpy;[22] thus per se, contributions from protonation effects will be minor under these conditions.

To reveal a closer match with the crystallographic data, we applied two distinct scenarios during the ITC titrations. In the first set of titrations, the ligand was directly titrated to the protein in the sample cell. In the second set, the 20-residue peptide inhibitor PKI (see above) was incubated with the protein and then the ligand added.

Accordingly, measurements were performed in the presence (triangle symbols) and absence (circular symbols) of the substrate-mimicking inhibitor peptide PKI (Figure 4).

Upon comparison of the relative differences of the two sets of thermodynamic profiles, it is apparent that on absolute scale an offset between both sets of profiles is given. This leads to a shift toward more favorable entropy and less beneficial enthalpy in the presence of PKI (triangles). Thus, the relative differences between the ligands correlate in both cases.

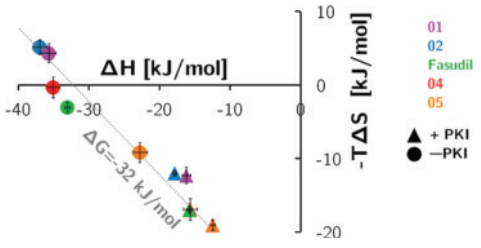

Figure 4. Thermodynamic profiles for all five ligands in absence (circles) and presence of PKI (triangles). The entropy contribution is displayed on the *y*-axis and enthalpy on the *x*-axis. The dotted line represents isoaffinity for the mean ΔG values of 32 kJ/mol. Titrations with the different ligands are colored according to the color-code presented in Figure 1. The triangular symbol for ligand **04** (red) is virtually hidden under the same profile as found for fasudil (green).

All five ligands bind to PKA with virtually the same affinity. Moreover, it is striking that the binding signatures of fasudil (green), the two methylpiperazine-substituted **01** (purple) and **02** (blue), and the open-chain ligand **04** (red) are similar and scatter maximally in $\Delta\Delta H$ = 4.2 kJ/mol and $-T\Delta\Delta S$ = 7.8 kJ/mol. In contrast, the long-chain ligand **05** (orange) displays a unique thermodynamic profile significantly reduced in its enthalpic and simultaneously enhanced in its entropic contribution to binding. In consequence, **05** is the most entropically and least enthalpically favored binder. In case of the presence of PKI, the effect concerning ligand **05** is similar but somewhat less pronounced.

Correlation of Amide Chemical Shift Perturbations in the Presence and Absence of PKI. To further analyze the structural influence of the peptidic inhibitor PKI, which is present in all of the studied crystal structures, $^{1}H^{15}N$ best-TROSY spectra of PKA were measured and the amide chemical shift perturbation (CSP) of 88 amino acids was determined for each ligand in the presence and absence of PKI (Figure S7A–C). Figure 5 shows the CSP for a selection of residues in the absence and presence of PKI for the five different ligands and the corresponding amide location in the X-ray structure. These data indicate similar binding properties of the ligands in the absence or presence of the PKI peptide and thus demonstrate the relevance of the crystal structures only determined in the presence of PKI.

The largest spatial difference can be observed for residues Gly55 (not assignable for the long-chain ligand **05**), Ala188, and Arg256 (Figure S7D). Gly55 is located in the Gly-loop, which is involved in the strongest induced-fit adaptations observed in the five crystal structures. Ala188 resides two amino acids C-terminal from the DFG motif and is in close proximity to the PKI-peptide's C-terminus. Arg256 is remote from the active site at the bottom of the large subunit located in close proximity to the N-terminus of the PKI peptide. The NMR data fully support and agree with the structural information from crystallographic analysis. The spatial alignment of the crystal structures in Figure 2 was performed using the backbone atoms of the residues with the smallest CSPs, thereby ensuring an unbiased alignment.

The Most Flexible Ligand Does Not Form a Flexible Protein–Ligand Complex. In order to analyze the residual flexibility of the resulting protein–ligand complexes ^{15}N T_2 relaxation NMR measurements were performed. These data (Figure S7D) indicate higher flexibility for the N-terminal 13 residues. The average values of the remainder ^{15}N T_2 relaxation values (75 of the 88 backbone amide signals that could be tracked reliably) are presented in Figure 6. The ^{15}N T_2 relaxation time can be used as a measure for backbone dynamics (a more rigid protein backbone will show a smaller ^{15}N T_2 relaxation time). On average, the dynamics of all five complexes are very similar. Interestingly, ligand **05** with the largest amount of internal degrees of freedom does not form a significantly more flexible protein–ligand complex compared to the other more constrained members of the series.

Protein Hydration with and without Fasudil or Ligand 05. Protein hydration can be conveniently monitored through NMR relaxometry, which provides the field dependence of the water proton longitudinal relaxation rates in protein solutions, in turn reflecting the dynamics of the proteins and the strength of the interactions between proteins

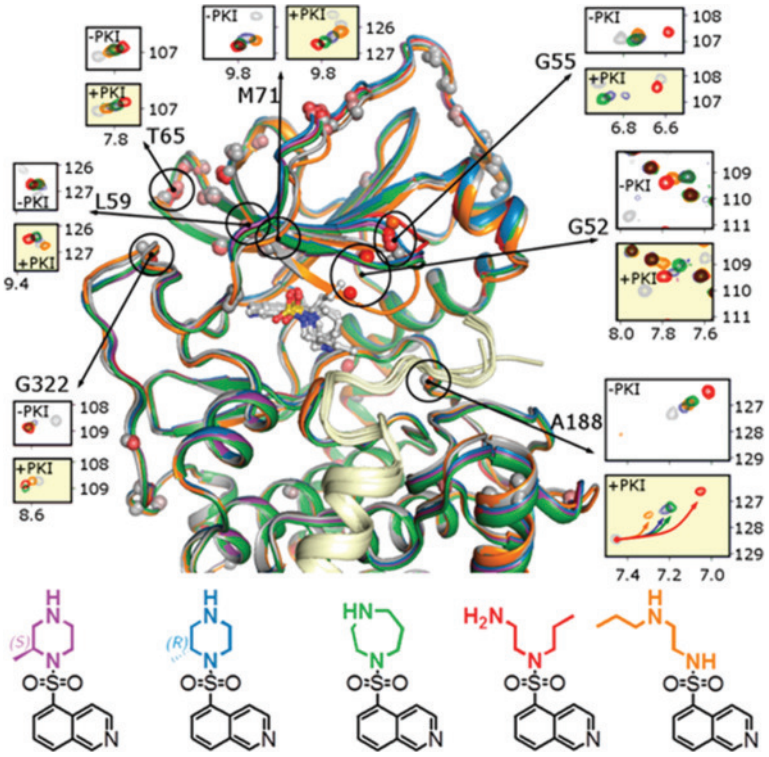

Figure 5. Amide chemical shift perturbations for a selection of residues and their corresponding location in the X-ray crystal structure. Sections from an overlay of $^{1}H^{15}N$ best TROSY spectra are shown for PKA with and without (gray) ligands in the presence and absence of the PKI. Ligands **01** (purple) and **02** (blue) show nearly identical CSPs.

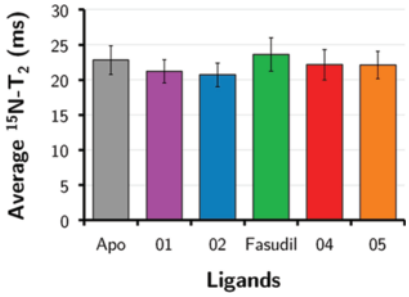

Figure 6. Average amide ^{15}N T_2 relaxation time for the PKA protein (75 out of 88 residues, excluding the flexible N-terminal residues) in the presence of the PKI peptide, with and without ligands. The overall differences are small. Error bars present the averaged standard deviation.

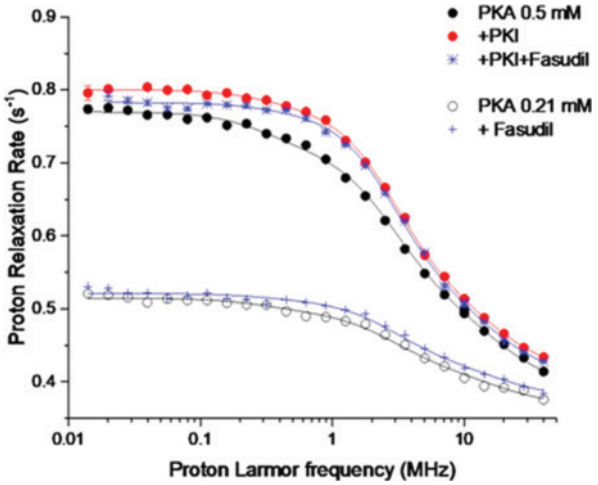

Figure 7. Water proton relaxometry profile of PKA with and without PKI and/or fasudil at 298 K. The lines are the best fit profiles calculated from the parameters reported in Table S5.

and water molecules.[23−26] NMR relaxometry is carried out with a dedicated instrument that provides the measurement of the nuclear longitudinal relaxation rates from 0.01 to tens of MHz, indicated NMRD profiles. These profiles report on the water proton spectral density functions, which depend on the superposition of the different motional processes, in turn associated with characteristic motional correlation times occurring on time scales from nanoseconds to microseconds.

Relaxometry measurements were performed at 298 K for PKA with and without the inhibitor peptide PKI and/or with and without fasudil (Figure 7). The data show that in the presence of PKI and/or fasudil the relaxation rates are slightly larger than for the free PKA samples. Furthermore, while the relaxation rates are basically constant at low fields in the presence of PKI and/or fasudil, the profiles for the free PKA samples show a slight decrease between 0.1 and 1 MHz. Consequently, the relaxometry profiles measured in the presence of PKI/fasudil can be nicely reproduced from the sum of two Lorentzian dispersions with different correlation times, whereas the profiles of free PKA require three Lorentzian dispersions. All profiles were thus fitted using eq 3,[23,24,27] and the best fit values are found in Table S5. Water molecules interacting with the protein or with the protein complexes as well as exchangeable protein protons contribute to the observed relaxation rates depending on the correlation

time modulating the dipole−dipole interactions. The effective correlation time for the different protons is the fastest between the reorientation time and the exchange time. The parameter a reports on the contribution to water relaxation from protons relaxing with correlation times smaller than few nanoseconds, whereas b_1, b_2, and b_3 report on the contributions from protons relaxing with correlation time τ_{slow}, τ_R (the protein reorientation time), and τ_{fast}, respectively, with τ_{fast} shorter than τ_R but larger than few nanoseconds. This correlation time can be due to fast local mobility at the protein site or to a water exchange rate faster than protein rotation. The contribution from protons relaxing with such a correlation time much shorter than τ_R is typically between 40% and 80% of the total.[24]

This fit shows that the contribution from protons relaxing with a correlation time τ_R = 28 ns or with a correlation time τ_{fast} = 5 ns slightly increases on passing from free PKA to PKA bound to PKI and/or fasudil, whereas the small amount of protons relaxing with a correlation time τ_{slow} = 240 ns decreases. The best fit value of τ_R (28 ns) is in good agreement with the value calculated with HYDRONMR[26] using the PDB structure 4WIH,[28] for which a correlation time of 26 ns is calculated. The presence of a decreased contribution from water molecules with correlation time τ_{slow} upon PKI and fasudil binding may suggest that in free PKA some aggregation is present and that the aggregated protein decreases/disappears in the presence of the ligands. Overall, the data indicate that the hydration of the protein does not decrease but rather slightly increases upon PKI and/or fasudil binding, although the difference is close to the error of the best fit values.

In addition, we investigated whether relaxometry could detect differences between the binding of fasudil and ligand **05** as a result of a larger number of water molecules removed from the active site upon ligand **05** binding than upon fasudil binding. This could possibly explain the entropic advantage found for **05** binding to PKA. We therefore collected relaxometry profiles of PKA in presence and absence of PKI with either ligand **05** or fasudil (Figure S8). These measurements show, however, that no differences can be detected between PKA + fasudil and PKA + ligand **05**. This clearly indicates that putative differences in the inventory of water displacement do not explain the entropic advantage of ligand **05** over fasudil.

Entropic Desolvation Contributions Investigated by Molecular Dynamics Simulation. In order to obtain insights of which additional molecular contributors to entropy are important in the current case, molecular dynamics (MD) simulations were carried out. We focused on fasudil and ligand **05** as experimental relaxometry data are available for these ligands indicating analogous hydration patterns for both protein−ligand complexes. Simulations were conducted for these two ligands, first, in their PKA-bound state in the presence of PKI and, second, in aqueous solution prior to protein binding in absence of the enzyme (details about the setup of the simulations are given in the Supporting Information, section 6). The MD simulations were subsequently used for an in-depth analysis of the ligand desolvation thermodynamics in aqueous solution. Finally, the simulation of the ligands in aqueous solution was compared to and validated with experimental NMR ROE distance information (taken from rotating frame NOEs) in order to obtain an idea about the predominantly populated conformers of the ligand in buffered aqueous solution.

Ligand Conformational Entropy Paradigm Confirmed by Simulation. At first, MD simulations of fasudil and **05** were conducted in their protein-bound states (each 100 ns), complemented by MDs in aqueous solution describing the ligands in their unbound solution state prior to protein binding (each 100 ns). These calculations were performed to estimate on the conformational entropy contributions of the ligand involving the transfer from aqueous solution to the protein-bound state. The conformational entropy difference for each of the two ligands between bound and unbound state was computed using CENCALC.[29] As anticipated by their chemical composition, the loss in conformational binding entropy contribution ($-T\Delta S_{conf}$) upon PKA binding is larger for ligand **05** than for fasudil (**05**, 9.3 ± 0.3 kJ/mol; fasudil, 4.8 ± 1.3 kJ/mol; see Table S7 in Supporting Information, all values calculated at 300 K), indicating a higher loss of flexibility upon binding of **05** over fasudil. As described above, the NMR spectroscopic measurements did not reveal major structural differences of PKA experienced upon binding of the two ligands including putative differences in the inventory of water displacement. Therefore, any contributions from the protein will not matter in a relative comparison of the two complexes. As a consequence, in our subsequent evaluations, we solely focused on the internal degrees of freedom of fasudil and **05**.

Calculation of Ligand Desolvation Entropy. The trajectories obtained from 100 ns unconstrained MD simulations of unbound fasudil and **05** in aqueous solution were clustered with *cpptraj* (V15, see section 6.2.3 in Supporting Information). The conformational ensemble found for fasudil can be well described by two, equally populated clusters (50.1% vs 49.9%) of closely related conformers. In contrast, conformational variance of **05** was best described using three clusters (67.8%, 18.4%, and 13.9%). Most interesting, the crystallographically observed conformation of **05** in the bound state is found in the least populated cluster.

The best representative conformers for each cluster were then used as starting geometries for follow-up MD simulations but now applying positional restraints so that the conformations of the cluster representatives were preserved throughout the simulations. This fixation of internal degrees of freedom is necessary to subsequently perform an evaluation of the solvation pattern around the ligands using the GIST method (grid inhomogeneous solvation theory) as a postprocessing procedure.[30,31] The latter approach calculates solvation thermodynamic quantities, such as entropy, and maps them on a three-dimensional grid for graphical evaluation.

Visual inspection of the GIST entropy maps revealed that the secondary amino group is well solvated for both ligands fasudil and **05** (Figure 8). The desolvation of this group would be entropically beneficial, since solvent hydrogen-bonding interactions result in both translational and orientational restrictions of the entrapped water molecules. On the contrary, the sulfonamide nitrogen atom is less well solvated in fasudil (Figure 8A) compared to **05** (Figure 8B) for all clusters. This is probably enhanced by the pseudo-macrocyclic back-folded shape of the predominant conformers of **05** (Figure 8B1,B2), which assist in binding water molecules more tightly to the sulfonamide group. Consequently, the predominantly populated conformations of ligand **05** lead to an increase of the probability to find a water molecule in the vicinity of the solvated ligand and therefore increases the entropy difference

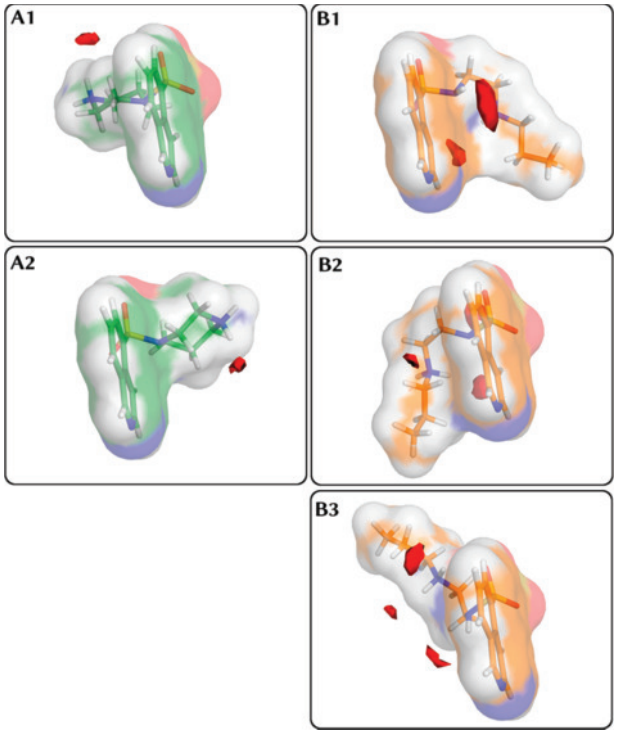

Figure 8. (A1, A2) Cluster centroids for the two conformational clusters of fasudil, which are populated in 50.1% and 49.9% of the MD ensemble, respectively. (B1, B2, B3) Cluster centroids of **05**, populated in 67.8%, 18.4%, and 13.9% of the MD ensemble. The red isosurface displays solvent entropy at −2.5 (kJ/mol)/Å^3.

between ligand-entrapped water molecules and those in bulk solvent phase.

To quantify these differences, we determined the solvation enthalpy ΔH^0 and entropy ΔS^0. They are obtained as weighted sum of the GIST calculations using N cluster representatives as obtained from the conformational clustering of the MD trajectory (eq 2):

$$\langle \Delta A^0 \rangle = \sum_i^N p(q_i)\, \Delta A^0(q_i); \quad A^0 \text{ is enthalpy or entropy} \tag{2}$$

Here, $p(q)$ is the probability of finding the solvated ligand in conformation q_i (i.e., the occupancy of a conformational cluster, cf. Figure 8) and the Δ indicates that all quantities A^0 are calculated with respect to bulk solvent state. The solvation quantities in the vicinity of the solvated ligand can be accessed quantitatively by spatially summing ΔA^0 over a volume that captures the first layer of solvation of the ligand (background of the method is found in section 6.1.4 of the Supporting Information).

Due to the enhanced hydrogen-bonding properties of the sulfonamide group in ligand **05** in the predominantly populated pseudo-macrocyclic back-folded conformers, increased solvation entropy contributions are suggested in comparison to fasudil (Table 1). A difference in $-T\Delta S_{tot}$ at 300 K between **05** and fasudil is computed to 15.2 ± 0.7 kJ/mol. With respect to the solvation free energy ΔG, no significant difference between both ligands can be assigned within the error bars of the calculations. Due to error propagation of the large individual energy contributions, the uncertainty in the ΔG difference becomes rather sizable. Since ligand **05** and fasudil do not differ in their experimentally determined binding affinities, our calculation is supported by the fact that, overall, the price for the desolvation free energy should be indistinguishable for both ligands.

Table 1. Different Solvation Thermodynamic Properties and Conformational Entropy Difference for the Ligand during Binding, As Obtained from GIST and CC-MLA Calculations at 300 K[a]

ΔA [kJ/mol]	fasudil	ligand **05**	Δ[b]
$-T\Delta S_{conf}$	4.8 ± 1.4	9.3 ± 0.3	4.5 ± 1.4
$-T\Delta S_{orient}$	41.5 ± 0.1	48.0 ± 0.2	6.5 ± 0.3
$-T\Delta S_{trans}$	53.5 ± 0.3	62.2 ± 0.2	8.7 ± 0.4
$-T\Delta S_{tot}$	95.1 ± 0.6	110.2 ± 0.4	15.1 ± 0.7
ΔE_{ww}	360.1 ± 5.9	367.6 ± 4.1	7.5 ± 7.2
ΔE_{sw}	−328.1 ± 5.7	−343.7 ± 3.6	−14.8 ± 6.7
ΔE_{tot}	31.1 ± 8.3	23.9 ± 5.5	−7.2 ± 9.9
ΔG	126.3 ± 8.3	134.2 ± 5.5	7.9 ± 9.9

[a]The uncertainty reported for each value is the ±standard deviation from the mean. [b]This column reports the differences between ligand **05** and fasudil.

Combined NMR Experiments and MD Simulations. To validate the findings suggested by our MD simulations in aqueous solution, we consulted NMR experiments. The water molecules trapped by ligand **05** in buffer solution cannot be characterized by NMR directly, due to the fast exchange rate of ligand-trapped water molecules. It is assumed that the solvated ligand perturbs the otherwise homogeneous solvent and therefore gives rise to enhanced solvent structuring. Following this rationale, the match of the in silico ensemble with an experimentally observed conformational ensemble would strongly indicate that the proposed water entrapment takes place in solution and leads to the above-computed favorable solvation entropy. For this, we analyzed our unconstrained MD simulation of **05** in water and compared it to NMR-observed ROE distances. Since a particular distribution of these distances can be realized by more than one conformational ensemble, we performed additional MD simulations with **05** but now applying NMR-derived distance potentials of varying strength. Important enough, no significant differences have been recorded for our unconstrained, unbiased simulations and the simulations applying NMR-based distance restraints (details on these simulations can be found in section 6.2.5 of the Supporting Information, including the 36 MD simulations with deviating settings of the distance potentials). We therefore believe that the conformational distributions found by the simulations are well representative of the conformational properties of fasudil and **05** in aqueous solution.

The trajectory that agreed best with experimental data (91% within experimental boundaries) was used for a principle component analysis (PC) of the conformational space. An overlap of 0.51 was found with the in silico ensemble (section 6.2.5 in Supporting Information), which is quite promising considering the high dimensionality of the conformation space compared to the PC subspace. Since subspace overlap can be obscured by different effects, the significance of the result was further assessed by its Z-score.[32] The Z-score is constructed by comparing the actual overlap to the overlap with a background model consisting of 500 random trajectories. Positive values indicate high significance, and zero or negative values indicate insignificant overlap. The calculated Z-score in the present case

is 5.84 and therefore indicates that similarity between the experimental ROE-derived ensemble and the in silico generated main cluster of **05** is far above noise and therefore can be assumed significant for our attempted analysis of the conformation and solvation properties.

DISCUSSION

For a series of five congeneric and nearly equipotent ligands, studied in this contribution, we thoroughly analyzed the interactions with PKA. High-resolution crystallographic data revealed a comparable hinge binding mode of all ligands. As special feature, a strong induced-fit mechanism for ligand **05** (orange) is observed. NMR chemical shift perturbation data reveal high similarity between the structural properties of the different complexes in crystalline and solution state. NMR relaxation measurements unraveled the structural influence of inhibitor peptide PKI on the protein and allowed analysis of the backbone dynamics, which, however, agree across all studied complexes. Thermodynamic signatures were measured either in the absence or in the presence of the substrate mimicking peptide PKI. Even though all ligands bind with nearly the same affinity, they distinctly factorize in enthalpy and entropy. This also uncovers that the most flexible ligand **05** with the largest amount of internal degrees of freedom is, on first sight paradoxical and quite counterintuitive, the entropically most favored binder of the series, independent of the presence or absence of PKI. Usually, the binding of more rigid and conformationally preorganized ligands reveals an entropic advantage to binding.[33,34] In the present case, this would be expected for the ligands fasudil, **01**, and **02** possessing the conformationally restricted cyclic substituents.

It is remarkable that the relative differences in the thermodynamic profiles between the five ligands remain similar to each other in presence or absence of the substrate-like PKI. However, the overall shift of all profiles on absolute scale toward more entropy-favored binding appears reasonable upon binding of the substrate peptide as the protein becomes prestabilized and structurally organized in a way to better recognize the cosubstrate ATP or, in our case, the inhibitors of the fasudil-type. The thermodynamic profiles of ligand binding are all shifted toward an entropically more favorable but enthalpically less beneficial signature in the presence of PKI. This profile is in accordance with a better preorganization of one of the binding partners, here of the recipient protein.

Among the individual ligands, the entropically more favored binding of the conformationally less restricted ligand **05** to PKA could result (i) from the formation of a protein−ligand complex with strongly enhanced residual flexibility, (ii) from increased displacement of active-site water molecules upon ligand binding to the uncomplexed protein, or (iii) from a difference in the solvation properties among the five ligands in aqueous solution prior to binding. These contributions must even overcompensate the entropic losses to be paid by restricting the conformational flexibility of ligand **05** to the bound state. Calculations, which evaluate the entropic losses for the spatial restriction of the more rigid fasudil in comparison to the more flexible ligand **05** upon the transfer to the bound state, confirm this assumption.

The first aspect, listed above, suggests the formation of a complex of enhanced residual flexibility. We suppose that this is unlikely, as ligand **05** shows overall the lowest *B*-factors in the crystal structure. It reflects the lowest residual mobility in bound state in the series (Table S2), which correlates with a strong induced-fit adaptation, pulling the Gly-loop toward the bound ligand. Our hypothesis is further supported by the NMR relaxation data, which do not indicate enhanced mobility for the complex with this ligand compared to the others. Clearly, these findings do not speak for an entropic advantage of ligand **05** upon binding.

A second putative explanation for the favorable entropy contribution of **05** would originate from the displacement of a larger amount of previously well-ordered active-site water molecules upon protein−ligand complex formation. Unfortunately, the amount of water molecules in the active site cannot be reliably evaluated for the entire series by crystallography due to a less well-defined electron density in this area in consequence of enhanced loop flexibility. However, NMR relaxometry measurements show that there is no significant difference in the hydration pattern between the complexes formed with **05** and fasudil. Thus, we believe that also differences in the amount of displaced water molecules cannot explain the entropic advantage of the more flexible ligand **05**.

A third alternative explanation, additionally influencing the thermodynamic signature of ligand **05** compared to the other members of the series, can arise from differences of the ligands in aqueous solution prior to PKA binding. Remarkably, this effect has nothing to do with the actual binding to the protein. Once the ligands are released from the bulk water phase and accommodate in the protein, they have to shed their solvation shells. If these shells show structural differences in the local hydration pattern, deviating thermodynamic signatures will result. Indeed MD simulations strongly indicate that the entropically beneficial signal of ligand **05** is due to a unique hydration pattern triggered by a back-folded conformation that favorably entraps water molecules. The frequent occurrence of this conformation (68% of the time) in aqueous solution was confirmed within the boundaries of NMR spectroscopic data (ROE distances).

Overall our calculations suggest that the entropic losses, required to immobilize the more flexible ligand **05** compared to fasudil in the binding pocket of PKA, are overcompensated by the entropic advantage resulting from the water release once ligand **05** is desolvated. Nevertheless, we are careful comparing such values quantitatively on a common scale including our microcalorimetry data, since the methodologies of the applied methods to estimate such values differ strongly.

Our experimental data demonstrate that the entropically more favored binding of **05** to the protein mainly results from an entropic benefit of the ligand while shedding its hydration shell upon leaving the bulk water phase. Our hypothesis that a ligand with a larger amount of internal degrees of freedom does not necessarily lead to entropically less-favored binding was also observed in other cases but without providing a conclusive explanation.[35] Therefore, the assumption that the number of the ligand's degrees of freedom to be lost upon complex formation has always a dominating impact on the entropic binding component needs to be questioned or at least requires a more detailed analysis of the binding event as a whole. It demonstrates that simple design guidelines cannot be generalized unreflectively and deserve a much more careful consideration. In particular, the frequently neglected factor of ligand solvation has to be more thoroughly considered.

CONCLUSION

Commonly applied design guidelines need to be systematically investigated and assessed for different protein and ligand

classes. Rules that hold for small and rigid proteins do not necessarily apply for larger or flexible proteins. From our systematic study on a protein kinase we conclude that the thermodynamic profile is not dominated by the loss of degrees of freedom due to fewer rotatable bonds on the ligand. The hypothesis that ligand rigidification necessarily results in an overall significantly more entropic binding profile could not be confirmed. Strikingly, we even recorded the opposite trend in that the most flexible ligand was the most favored entropic binder. Therefore, the loss of degrees of freedom of the ligand, which, as a matter of fact, has to be paid, does not necessarily dominate the thermodynamic profile. Even in the present case of binding to a flexible protein like a kinase, the effect of residual flexibility of the formed protein−ligand complex appears to be minor as all complexes under consideration show very similar NMR relaxation data. In fact, the predominant effect seems to result from structural differences in the hydration pattern of the ligands in the bulk water phase prior to any protein binding. They appear to determine the resulting entropically more favored binding signal.

In summary, our results indicate that the complexity of structure−activity relationships increases with protein flexibility and desolvation differences of either the active site or the ligand molecules. Most strikingly, these contributions cannot be treated as orthogonal design parameters in rational optimization of potential drug candidates. Our data indicate that global understanding and reliable predictions of thermodynamic profiles need a comprehensive view on the binding event and require many more systematic studies of congeneric ligand series.

EXPERIMENTAL SECTION

Protein Expression and Purification for ITC and Crystallization. The catalytic subunit of cAMP-dependent protein kinase from Chinese hamster (Cricetulus griseus; UniProt ID P25321) cells (98% sequence identity with human isoform) was expressed with a His-tag in a modified pET16b-vector with an introduced TEV-cleavage site between the protein N-terminus and His-tag. This plasmid was transformed into *E. coli* strain *BL21 (DE3)/pLysS* (Novagen).[28]

Cell disruption was performed using a high-pressure homogenizer for multiple cycles. After centrifugation (1 h at 30 000*g*) cell lysate supernatant was purified in a first step using a Ni-NTA column that binds the His-tag of the protein and was eluted by an imidazole gradient. The His-tag was then cleaved off by TEV-protease. Afterward, an inverse Ni-NTA column was employed collecting PKA in the flow-through. Finally, ion exchange chromatography was performed using a MonoS column separating 3-fold phosphorylated PKA from the 4-fold phosphorylated form using a HEPES buffer with a sodium chloride gradient.[28]

Protein Expression and Purification for NMR. The catalytic subunit of cAMP-dependent protein kinase was expressed, isotope labeled (^{15}N), and purified as previously described.[36]

Crystallization. Cocrystallization was performed using the hanging drop method at 277 K. The crystallization drops were composed as follows: 10 mg/mL PKA (240 μM), 30 mM MBT (MES/Bis-Tris buffer, pH 6.9), 1 mM DTT, 0.1 mM EDTA, 75 mM LiCl, 0.03 mM Mega 8, 0.07 mM PKI (Sigma, P7739), 1.2 mM ligand dissolved in DMSO from a 50−100 mM stock. The well contained a mixture of methanol in water with varying methanol concentrations (v/v) for the different ligands (fasudil, 18% methanol; ligand **05**, 18% methanol; ligand **04**, 14% methanol; ligand **01**, 16% methanol; ligand **02**, 19% methanol). In the crystallization setup streak-seeding was performed using a horse hair in order to initialize crystal growth. For crystal mounting, crystals were cryoprotected in 5 mM MBT (MES/Bis-Tris buffer, pH 6.9), 1 mM DTT, 0.1 mM LiCl, 1.2 mM ligand dissolved in DMSO from a 50−100 mM stock, 16% (v/v) methanol, 30% (v/v) MPD and flash-frozen in liquid nitrogen.

Crystal Structure Determination. All structures were collected at the electron storage ring Bessy II Helmholtz-Zentrum Berlin, Germany at beamline 14.1 on a Pilatus 6M pixel detector with resolutions between 1.42 and 1.62 Å. The data sets were processed using XDS,[37] and molecular replacement was performed using CCP4 Phaser[38] and PDB structure of PKA from *Bos taurus* 1Q8W as a model.[21] This was followed by simulated annealing, multiple refinement cycles of maximum likelihood energy minimization, and *B*-factor refinement using Phenix.[39] Coot[40] was used to fit amino acid side chains into σ-weighted $2F_o - F_c$ and $F_o - F_c$ electron density maps. If appropriate electron density was observed, multiple side chain conformations were built into the model and maintained during the refinement if the minor populated side chain displayed at least 20% occupancy. Hydrogen atoms were included using a riding model. Ramachandran plots for structure validation were generated using PROCHECK.[41] Data collection, unit cell parameters, and refinement statistics are given in the Supporting Information (Table S2). Analysis of temperature factors was performed with Moleman.[42] Protein and PKI *B*-factors were anisotropically refined, and water *B*-factors were isotropically refined for all structures. R_{free} was calculated using 5% of all reflections which were randomly chosen and not used for the refinement. The required ligand restraint files were created using the Grade Web server (accessed Dec, 12, 2014; Feb, 27, 2015; Apr, 22, 2015; Dec, 16, 2015; Mar, 16, 2016).[43,44] For figure preparation Pymol was used.[45]

Isothermal Titration Calorimetry. The buffer used for the ITC experiments contained 30 mM sodium phosphate buffer, pH 7.2, 10 mM $MgCl_2$, 100 mM NaCl, 3% (v/v) DMSO. All measurements were repeated 3−5 times. Further buffers were used in order to check for protonation linkage. In these buffers, 30 mM sodium phosphate buffer was replaced by 30 mM HEPES and 30 mM triethanolamine (TEA), respectively (both at pH 7.2). Buffer dependency was tested for all measurements in the absence of PKI. For the measurements expressed, purified and dialyzed PKA was used in the ITC-measuring cell. A 15- to 20-fold higher concentrated ligand solution, diluted in dialysis buffer, was then stepwise injected to the protein solution during the measurement. All measurements were performed at 298 K. ITC data were analyzed using NITPIC and Sedphat.[46,47] Raw data and exact values and standard deviations for ΔG, ΔH and $-T\Delta S$ can be found in the Supporting Information (Tables S3, S4).

Compound purity was analyzed using quantitative nuclear magnetic resonance spectroscopy (qNMR) and in the case of deviation from 1:1 binding stoichiometry, ligand concentration was corrected accordingly. The purity of the used ligands was at or above 95%.

NMR Measurements. The NMR samples contained about 0.1−0.2 mM PKA protein, 20 mM sodium phosphate buffer (pH 6.5), 80 mM NaCl, and 2 mM TCEP (tris(2-carboxyethyl)phosphine) and 10% D_2O (for spectrometer lock). The NMR experiments were conducted at a temperature of 298 K on Bruker Avance 600, 800, and 950 MHz spectrometers equipped with cryogenic triple-resonance probes. For the PKA + PKI complex, titration experiments were performed in which the unlabeled PKI peptide was added until no significant changes were observed anymore in the ^{1}H^{15}N-HSQC spectra after the last addition. The samples of PKA with PKI contained a slight excess of the PKI peptide, and the samples with the ligands contained a 5 times excess of the ligand to ensure the full complex formation. NMR spectra were acquired and processed using Topspin version 3.2 (Bruker Biospin) and analyzed using Sparky 3.114 (T. D. Goddard and D. G. Kneller, University of California, San Francisco). Resonances for the PKA protein have been assigned before.[36,48] The spectra of PKA alone, PKA with PKI, PKA with ligands, and PKA with PKI and ligands have been assigned by overlaying the ^{1}H^{15}N-HSQC spectra. Only the backbone amide signals that could be tracked reliably were further analyzed. Heteronuclear ^{15}N T_2 relaxation experiments were performed on the uniformly ^{15}N labeled PKA protein in complex with PKI with and without ligands. The relaxation rates were determined from a series of

spectra with delays of 0, 16.96, 33.92, 50.88, and 67.84 ms. The amide chemical shift perturbations (CSPs) were acquired from $^{1}H^{15}N$-best-TROSY[49] spectra.

Relaxometry. Water ^{1}H NMRD profiles were obtained by measuring the water proton relaxation rates, R_1, as a function of the applied magnetic field. The NMRD profiles were measured with a SPINMASTER2000 fast field cycling relaxometer (Stelar, Mede (PV), Italy) operating in the 0.01−40 MHz proton Larmor frequency range, at 298 K. The measurements are affected by an error of about ±1%, when fitted to a monoexponential decay/recovery of the magnetization in the field cycling experiment. Measurements were performed either in the presence or in the absence of PKI, with and without fasudil and with and without ligand **05**. Protein concentrations were 0.5 mM and 0.21 mM in the absence of PKI and 0.5 mM when PKI was added. Ligand concentration was 4−6 times larger than the protein concentration.

The profiles were fit using eq 3, where protons are assumed in fast exchange and the model-free approach is applied:[23,24,27]

$$R_1 = (0.3 + a) + b_1 J(\tau_{slow}) + b_2 J(\tau_R) + b_3 J(\tau_{fast}) \quad (3)$$

with $J(\tau) = 0.2\tau/[1 + (\omega\tau)^2] + 0.8\tau/[1 + (2\omega\tau)^2]$ and where a, b_1, b_2, b_3, τ_{slow}, τ_R, τ_{fast} are fitting parameters. In order to reduce the covariance among the many fit parameters, all profiles were fit simultaneously by imposing common values for τ_{slow}, τ_R, and τ_{fast} in the absence of PKI and τ_R and τ_{slow} values 5.4% larger in the presence of PKI (due to the estimated slower reorientation time of the complex upon PKI binding).

Molecular Dynamics Calculations. Details about the settings of our molecular dynamics simulations and the applied GIST calculations to estimate the effects of ligand hydration are documented in detail in the Supporting Information, section 6.

Ligands. Ligands **03**, **04**, and **05** were purchased from Uorsy (Ukraine). The *R* and *S* isomers of the 2-methylpiperazine inhibitors **01** and **02** were synthesized starting from 5-(chlorosulfonyl)-isoquinoline hydrochloride, prior to this freshly prepared from isoquinoline-5-sulfonic acid via a known literature procedure,[50,51] which was reacted with the respective, commercially available, enantiomerically pure *R* or *S*-configured mono-*N*-Boc-protected 3-methylpiperazine, thus rendering the corresponding inhibitor precursors, respectively. Finally, *N*-Boc deprotection with 4 M HCl in dioxane gave rise to the corresponding inhibitors **01** and **02** as their hydrochloride salts. We performed qNMR measurements to check the purity of our ligands which exceeded 95% purity.

■ ASSOCIATED CONTENT

Supporting Information

The Supporting Information is available free of charge on the ACS Publications website at DOI: 10.1021/acs.jmedchem.8b00105.

Crystallographic tables, pictures of the $mF_o - DF_c$ densities of all five ligands, NMR spectra of the ligands, qNMR data, ITC titration curves, amide CSPs and ^{15}N T_2 relaxation per amino acid, synthesis protocols, analytical data, MD simulations and GIST calculations to derive thermodynamic quantities, MD simulations with NMR distance potentials, and comparison of MD and NMR ensembles in Cartesian and distance space (PDF)

Molecular formula strings (CSV)

Accession Codes

Atomic coordinates and experimental details for all new crystal structures will be released in the PDB upon publication: PKA−ligand **01**, 5LCU; PKA−ligand **02**, 5LCT; PKA−fasudil, 5LCP; PKA−ligand **04**, 5LCR; PKA−ligand **05**, 5LCQ.

■ AUTHOR INFORMATION

Corresponding Authors

*H.S.: e-mail: schwalbe@nmr.uni-frankfurt.de.

*G.K.: e-mail, klebe@staff.uni-marburg.de; phone, +49 6421 28 21313.

ORCID

Harald Schwalbe: 0000-0001-5693-7909

Gerhard Klebe: 0000-0002-4913-390X

Author Contributions

B.W.-S. performed expression, crystallization, crystal structure analyses, and ITC. H.R.A.J., K.S., D.K., and S.S. expressed protein, measured CSP and ^{15}N T_2 relaxation times. G.P. and C.L. contributed relaxometry measurements. T.W. performed the MD and GIST calculations. H.-D.G. synthesized the ligands. A.H., H.S., and G.K. helped interpret the data. All authors wrote the manuscript. All authors have given approval to the final version of the manuscript.

Notes

The authors declare no competing financial interest.

■ ACKNOWLEDGMENTS

We acknowledge funding from the European Research Council (ERC) of the European Union, Project 268145 (DrugProfilBind) and the LOEWE Research Cluster SynChemBio of the Federal State of Hesse (Germany). Furthermore, we acknowledge travel support from and synchrotron beamtime at BESSY II Helmholtz-Zentrum Berlin in Berlin/Germany and from Instruct-ERIC, a Landmark ESFRI project, and specifically, CERM/CIRMMP Italy center. Computational resources and technical support were provided by HRZ Marburg. Furthermore, we acknowledge support from the EC contract # 653706 (iNext).

■ ABBREVIATIONS USED

PKA, cAMP-dependent protein kinase; ITC, isothermal titration calorimetry; NMR, nuclear magnetic resonance spectroscopy; CSP, chemical shift perturbation; TROSY, transverse relaxation optimized spectroscopy; MBT, Mes/Bis-Tris; DTT, dithiothreitol; EDTA, ethylenediaminetetraacetic acid; MPD, 2-methyl-2,4-pentanediol; DMSO, dimethyl sulfoxide; TEA, triethanolamine; qNMR, quantitative nuclear magnetic resonance spectroscopy; PDB, Protein Data Bank; PKI, protein kinase inhibitor; DFG, aspartate-phenylalanine-glycine motif; Gly, glycine; Ala, alanine; Asp, aspartate; Thr, threonine; Glu, glutamate; Arg, arginine; Ser, serine; Val, valine; Cys, cysteine; ATP, adenosine triphosphate; MD, Molecular Dynamics; GIST, Grid Inhomogeneous Solvation Theory

■ REFERENCES

(1) Freire, E. Do enthalpy and entropy distinguish first in class from best in class? *Drug Discovery Today* **2008**, *13*, 869−874.

(2) Kawasaki, Y.; Freire, E. Finding a better path to drug selectivity. *Drug Discovery Today* **2011**, *16*, 985−990.

(3) Núñez, S.; Venhorst, J.; Kruse, C. G. Target-drug interactions: first principles and their application to drug discovery. *Drug Discovery Today* **2012**, *17*, 10−22.

(4) Klebe, G. Applying thermodynamic profiling in lead finding and optimization. *Nat. Rev. Drug Discovery* **2015**, *14*, 95−110.

(5) Tarcsay, Á.; Keserü, G. M. Is there a link between selectivity and binding thermodynamics profiles? *Drug Discovery Today* **2015**, *20*, 86−94.

(6) Bertini, I.; Calderone, V.; Fragai, M.; Giachetti, A.; Loconte, M.; Luchinat, C.; Maletta, M.; Nativi, C.; Yeo, K. J. Exploring the subtleties of drug- receptor interactions: the case of matrix metalloproteinases. *J. Am. Chem. Soc.* **2007**, *129*, 2466−2475.
(7) Ladbury, J. E.; Klebe, G.; Freire, E. Adding calorimetric data to decision making in lead discovery: a hot tip. *Nat. Rev. Drug Discovery* **2010**, *9*, 23−27.
(8) Mann, A. In *The Practice of Medicinal Chemistry*, 2nd ed. ed.; Wermuth, C. G., Ed.; Academic Press: London, 2003; pp 233 − 250.
(9) Loughlin, W. A.; Tyndall, J. D. A.; Glenn, M. P.; Fairlie, D. P. Beta-strand mimetics. *Chem. Rev.* **2004**, *104*, 6085−6117.
(10) Chang, C. A.; Chen, W.; Gilson, M. K. Ligand configurational entropy and protein binding. *Proc. Natl. Acad. Sci. U. S. A.* **2007**, *104*, 1534−1539.
(11) Chaires, J. B. Calorimetry and thermodynamics in drug design. *Annu. Rev. Biophys.* **2008**, *37*, 135−151.
(12) Borsi, V.; Calderone, V.; Fragai, M.; Luchinat, C.; Sarti, N. Entropic contribution to the linking coefficient in fragment based drug design: a case study. *J. Med. Chem.* **2010**, *53*, 4285−4289.
(13) Wong, C. F. Flexible ligand-flexible protein docking in protein kinase systems. *Biochim. Biophys. Acta, Proteins Proteomics* **2008**, *1784*, 244−251.
(14) Huang, Z.; Wong, C. F. Conformational selection of protein kinase A revealed by flexible-ligand flexible-protein docking. *J. Comput. Chem.* **2009**, *30*, 631−644.
(15) Kornev, A. P.; Taylor, S. S. Dynamics-driven allostery in protein kinases. *Trends Biochem. Sci.* **2015**, *40*, 628−647.
(16) Olsson, T. S. G.; Williams, M. A.; Pitt, W. R.; Ladbury, J. E. The thermodynamics of protein-ligand interaction and solvation: insights for ligand design. *J. Mol. Biol.* **2008**, *384*, 1002−1017.
(17) Gilson, M. K.; Liu, T.; Baitaluk, M.; Nicola, G.; Hwang, L.; Chong, J. BindingDB in 2015: a public database for medicinal chemistry, computational chemistry and systems pharmacology. *Nucleic Acids Res.* **2016**, *44*, D1045−D1053.
(18) Manning, G.; Whyte, D. B.; Martinez, R.; Hunter, T.; Sudarsanam, S. The protein kinase complement of the human genome. *Science* **2002**, *298*, 1912−1934.
(19) Shibuya, M.; Asano, T.; Sasaki, Y. In *Cerebral Vasospasm*; Seiler, R. W., Steiger, H.-J., Eds.; Springer: Vienna, 2001; pp 201−204.
(20) Sasaki, Y.; Suzuki, M.; Hidaka, H. The novel and specific Rho-kinase inhibitor (S)-(+)-2-methyl-1-[(4-methyl-5-isoquinoline)-sulfonyl]-homopiperazine as a probing molecule for Rho-kinase-involved pathway. *Pharmacol. Ther.* **2002**, *93*, 225−232.
(21) Breitenlechner, C.; Gassel, M.; Hidaka, H.; Kinzel, V.; Huber, R.; Engh, R. A.; Bossemeyer, D. Protein kinase A in complex with Rho-kinase inhibitors Y-27632, fasudil, and H-1152P: structural basis of selectivity. *Structure* **2003**, *11*, 1595−1607.
(22) Goldberg, R. N.; Kishore, N.; Lennen, R. M. Thermodynamic quantities for the ionization reactions of buffers. *J. Phys. Chem. Ref. Data* **2002**, *31*, 231.
(23) Venu, K.; Denisov, V. P.; Halle, B. Water 1H magnetic relaxation dispersion in protein solutions. a quantitative assessment of internal hydration, proton exchange, and cross-relaxation. *J. Am. Chem. Soc.* **1997**, *119*, 3122−3134.
(24) Bertini, I.; Fragai, M.; Luchinat, C.; Parigi, G. 1H NMRD profiles of diamagnetic proteins: a model-free analysis. *Magn. Reson. Chem.* **2000**, *38*, 543−550.
(25) Ravera, E.; Parigi, G.; Mainz, A.; Religa, T. L.; Reif, B.; Luchinat, C. Experimental determination of microsecond reorientation correlation times in protein solutions. *J. Phys. Chem. B* **2013**, *117*, 3548−3553.
(26) Garcia de la Torre, J.; Huertas, M.; Carrasco, B. HYDRONMR: prediction of NMR relaxation of globular proteins from atomic-level structures and hydrodynamic calculations. *J. Magn. Reson.* **2000**, *147*, 138−146.
(27) Ravera, E.; Fragai, M.; Parigi, G.; Luchinat, C. Differences in dynamics between crosslinked and non-crosslinked hyaluronates measured by using fast field-cycling relaxometry. *ChemPhysChem* **2015**, *16*, 2803−2809.
(28) Kudlinzki, D.; Linhard, V. L.; Saxena, K.; Sreeramulu, S.; Gande, S.; Schieborr, U.; Dreyer, M.; Schwalbe, H. High-resolution crystal structure of cAMP-dependent protein kinase from Cricetulus griseus. *Acta Crystallogr., Sect. F: Struct. Biol. Commun.* **2015**, *71*, 1088−1093.
(29) Suárez, E.; Diaz, N.; Méndez, J.; Suárez, D. CENCALC: a computational tool for conformational entropy calculations from molecular simulations. *J. Comput. Chem.* **2013**, *34*, 2041−2054.
(30) Nguyen, C. N.; Young, T. K.; Gilson, M. K. Grid inhomogeneous solvation theory: hydration structure and thermodynamics of the miniature receptor cucurbit[7]uril. *J. Chem. Phys.* **2012**, *137*, 044101.
(31) Nguyen, C. N.; Cruz, A.; Gilson, M. K.; Kurtzman, T. Thermodynamics of water in an enzyme active site: grid-based hydration analysis of coagulation factor Xa. *J. Chem. Theory Comput.* **2014**, *10*, 2769−2780.
(32) Velázquez-Muriel, J. A.; Rueda, M.; Cuesta, I.; Pascual-Montano, A.; Orozco, M.; Carazo, J.-M. Comparison of molecular dynamics and superfamily spaces of protein domain deformation. *BMC Struct. Biol.* **2009**, *9*, 6.
(33) Neeb, M.; Hohn, C.; Ehrmann, F. R.; Härtsch, A.; Heine, A.; Diederich, F.; Klebe, G. Occupying a flat subpocket in a tRNA-modifying enzyme with ordered or disordered side chains: favorable or unfavorable for binding? *Bioorg. Med. Chem.* **2016**, *24*, 4900−4910.
(34) Rühmann, E.; Rupp, M.; Betz, M.; Heine, A.; Klebe, G. Boosting affinity by correct ligand preorganization for the S2 pocket of thrombin: a study by isothermal titration calorimetry, molecular dynamics, and high-resolution crystal structures. *ChemMedChem* **2016**, *11*, 309−319.
(35) Martin, S. F.; Clements, J. H. Correlating structure and energetics in protein-ligand interactions: paradigms and paradoxes. *Annu. Rev. Biochem.* **2013**, *82*, 267−293.
(36) Langer, T.; Vogtherr, M.; Elshorst, B.; Betz, M.; Schieborr, U.; Saxena, K.; Schwalbe, H. NMR backbone assignment of a protein kinase catalytic domain by a combination of several approaches: application to the catalytic subunit of cAMP-dependent protein kinase. *ChemBioChem* **2004**, *5*, 1508−1516.
(37) Kabsch, W. XDS. *Acta Crystallogr., Sect. D: Biol. Crystallogr.* **2010**, *66*, 125−132.
(38) McCoy, A. J.; Grosse-Kunstleve, R. W.; Adams, P. D.; Winn, M. D.; Storoni, L. C.; Read, R. J. Phaser crystallographic software. *J. Appl. Crystallogr.* **2007**, *40*, 658−674.
(39) Adams, P. D.; Afonine, P. V.; Bunkóczi, G.; Chen, V. B.; Davis, I. W.; Echols, N.; Headd, J. J.; Hung, L. W.; Kapral, G. J.; Grosse-Kunstleve, R. W.; McCoy, A. J.; Moriarty, N. W.; Oeffner, R.; Read, R. J.; Richardson, D. C.; Richardson, J. S.; Terwilliger, T. C.; Zwart, P. H. PHENIX: a comprehensive Python-based system for macromolecular structure solution. *Acta Crystallogr., Sect. D: Biol. Crystallogr.* **2010**, *66*, 213−221.
(40) Emsley, P.; Lohkamp, B.; Scott, W. G.; Cowtan, K. Features and development of Coot. *Acta Crystallogr., Sect. D: Biol. Crystallogr.* **2010**, *66*, 486−501.
(41) Laskowski, R. A.; MacArthur, M. W.; Moss, D. S.; Thornton, J. M. PROCHECK: a program to check the stereochemical quality of protein structures. *J. Appl. Crystallogr.* **1993**, *26*, 283−291.
(42) Kleywegt, G. J.; Zou, J.-Y.; Kjeldgaard, M.; Jones, T. A. In *International Tables for Crystallography Vol. F: Crystallography of Biological Macromolecules*; Rossmann, M. G., Arnold, E., Eds.; Springer: Dordrecht, The Netherlands, 2001; pp 353−356.
(43) Smart, O. S., Womack, T. O., Sharff, A., Flensburg, C., Keller, P., Paciorek, W., Vonrhein, C., Bricogne, G. http://www.globalphasing.com.
(44) Bruno, I. J.; Cole, J. C.; Kessler, M.; Luo, J.; Motherwell, W. D. S.; Purkis, L. H.; Smith, B. R.; Taylor, R.; Cooper, R. I.; Harris, S. E.; Orpen, A. G. Retrieval of crystallographically-derived molecular geometry information. *J. Chem. Inf. Comput. Sci.* **2004**, *44*, 2133−2144.
(45) DeLano, W. L. The PyMOL molecular graphics system; 2002. http://pymol.org (accessed Dec 2015).

(46) Keller, S.; Vargas, C.; Zhao, H.; Piszczek, G.; Brautigam, C. A.; Schuck, P. High-precision isothermal titration calorimetry with automated peak-shape analysis. *Anal. Chem.* **2012**, *84*, 5066−5073.
(47) Houtman, J. C. D.; Brown, P. H.; Bowden, B.; Yamaguchi, H.; Appella, E.; Samelson, L. E.; Schuck, P. Studying multisite binary and ternary protein interactions by global analysis of isothermal titration calorimetry data in SEDPHAT: application to adaptor protein complexes in cell signaling. *Protein Sci.* **2007**, *16*, 30−42.
(48) Masterson, L. R.; Shi, L.; Tonelli, M.; Mascioni, A.; Mueller, M. M.; Veglia, G. Backbone NMR resonance assignment of the catalytic subunit of cAMP-dependent protein kinase A in complex with AMP-PNP. *Biomol. NMR Assignments* **2009**, *3*, 115−117.
(49) Favier, A.; Brutscher, B. Recovering lost magnetization: polarization enhancement in biomolecular NMR. *J. Biomol. NMR* **2011**, *49*, 9−15.
(50) Morikawa, A.; Sone, T.; Asano, T. 5-Isoquinolinesulfonamide derivatives. 2. Synthesis and vasodilatory activity of N-(2-amino-ethyl)-5-isoquinoline sulfonamide derivatives. *J. Med. Chem.* **1989**, *32*, 46−50.
(51) Makhija, M. T.; Kasliwal, R. T.; Kulkarni, V. M.; Neamati, N. De novo design and synthesis of HIV-1 integrase inhibitors. *Bioorg. Med. Chem.* **2004**, *12*, 2317−2333.